



Evolution of the Non-metallic Inclusions Influenced by Slag-Metal Reactions in Ti-Containing Ferritic Stainless Steel

YONG WANG, JIN-HYUNG CHO, TAE-SU JEONG, ANDREY KARASEV, WANGZHONG MU, JOO HYUN PARK, and PÄR G. JÖNSSON

Laboratory experiment and thermodynamic calculation for the Ti-containing 24 mass pct Cr ferritic stainless steel with a CaO-SiO₂-Al₂O₃-MgO system slag were performed to investigate the effect of slag addition on the inclusion characteristics in molten steel. The morphology, composition, and size evolution of inclusions in steel samples were analyzed in three-dimensional by the electrolytic extraction method and in two-dimensional by the automatic analysis method. The results showed that the Ti content significantly decreased after the slag addition. However, the change of the Si content showed an opposite tendency. The decrease of the Ti content in steel was due to the reduction of SiO₂ and Al₂O₃ in the slag by dissolved Ti in steel. An increase of the TiO₂ content in the slag can decrease the Ti loss in steel based on the slag-steel kinetic analysis. The total O content in the steel melt decreased from 62 to 26 ppm, and the steel cleanliness was improved, since the number density of inclusions decreased after the slag refining. The results of a kinetic analysis showed that the rate-determining step of the oxidation of Ti in the steel and the reduction of SiO₂ in the slag were the mass transfer on the slag side. In addition, high Ti₂O₃-containing inclusions were found to be transformed to Cr₂O₃-Ti₂O₃-Al₂O₃ and Cr₂O₃-Ti₂O₃-SiO₂ system inclusions after the slag addition. The Al₂O₃ contents in inclusions increased while the Ti₂O₃ contents decreased with time. However, there were some amount of high melting point inclusions with high Al₂O₃ content, which were not what we expected. When plotted on logarithmic scales, the mole ratio $X_{Al_2O_3}/(X_{Ti_2O_3} \cdot X_{Cr_2O_3})$ values of the inclusions were expressed as a linear function of the $a_{Al}^2/(a_{Ti}^2 \cdot a_{Cr}^2 \cdot a_O^3)$ values of the steel melts with a slope of unity, which was theoretically expected.

<https://doi.org/10.1007/s11663-021-02314-3>
© The Author(s) 2021

I. INTRODUCTION

TITANIUM-CONTAINING ferritic stainless steels are widely used in various applications which require both high-temperature mechanical properties and excellent oxidation and corrosion resistance in an

aggressive environment.^[1] However, the presence of non-metallic inclusions, *i.e.*, titanium oxides and nitrides, caused by the alloy addition can seriously affect the production process as well as the quality of the final steel products, for example, clogging of the submerged entry nozzle.^[2,3] Normally, inclusions need to be removed or modified to achieve the optimal steel properties. The objective of inclusion modification techniques is to convert the existing solid inclusions to liquid inclusions that can be removed by coalescence and floatation.^[4,5] Further, liquid inclusions would be easy to deform thus preventing failure during casting and rolling.^[6–8] Therefore, it is crucial to control the formation of oxide inclusions in Ti-containing stainless steel during the steelmaking process.

For inclusions in Ti-stabilized ferritic stainless steels, many studies focused on the behaviour of Al₂O₃, Al₂O₃-TiO_x, MgO-Al₂O₃-TiO_x and TiN inclusions at different refining and casting stages.^[1,9,10] Calcium treatment of Ti-bearing inclusions in steel contributes

YONG WANG, ANDREY KARASEV, WANGZHONG MU, and PÄR G. JÖNSSON are with the Department of Materials Science and Engineering, KTH Royal Institute of Technology, Brinellvägen 23, 100 44 Stockholm, Sweden. Contact e-mail: yongwang@kth.se
JIN-HYUNG CHO and TAE-SU JEONG are with the Department of Materials Science and Engineering, Hanyang University, Ansan 15588, Korea. JOO HYUN PARK is with the Department of Materials Science and Engineering, KTH Royal Institute of Technology, and also with the Department of Materials Science and Chemical Engineering, Hanyang University. Contact e-mail: basicity@hanyang.ac.kr

Manuscript submitted 5 May 2021; accepted 30 August 2021.

Article published online September 27, 2021.

to the production of high-quality steel with fewer defects caused by inclusions.^[11,12] Li *et al.*^[9,13] and Chen *et al.*^[14] have shown that a small amount of Ca in Al-killed Ti-bearing stainless steel effectively modified $\text{Al}_2\text{O}_3\text{-TiO}_x$ inclusions into liquid oxides and reduced the stability of the spinel by modifying the solid Al_2O_3 inclusions into liquid calcium aluminates. Seo *et al.*^[15] investigated the effect of the Ca and Ti addition sequence on the inclusion behavior in Al-killed Ti-bearing stainless steels. They reported that a Ca treatment after the Ti addition was not an effective way to minimize the spinel formation. However, a Ca treatment before the Ti addition efficiently prevented the formation of MgAl_2O_4 spinel because of the depletion of available Al_2O_3 by the earlier Ca operation. Kruger *et al.*^[3] reported that the spinel inclusions were modified to spherical dual-phase spinel-liquid matrix inclusions by Ca treatment in a Ti-stabilized 11 mass pct Cr (409) stainless steel, which eliminated the clogging of SEN for this grade. In summary, these studies have investigated the effect of a Ca treatment on the modification of inclusions in molten steel.

Meanwhile, it is well known that the refining slag having a proper composition and excellent physico-chemical properties can effectively modify and remove the inclusions.^[16–23] It is a significant advantage that a good contact between metal and slag makes the steel chemically refined.^[24] Park *et al.*^[25] investigated the effect of $\text{CaO-Al}_2\text{O}_3\text{-MgO}$ slags on the formation of $\text{MgO-Al}_2\text{O}_3$ inclusions in a Si deoxidized 16 mass pct Cr ferritic stainless steel. They found that the MgO -rich spinel solid solutions were formed in the steel melt equilibrated with the highly basic slags saturated by CaO or MgO . Later, Park *et al.*^[10] also investigated the equilibrium between $\text{CaO-SiO}_2\text{-MgO-Al}_2\text{O}_3\text{-CaF}_2\text{-TiO}_2$ slag and a Si deoxidized Ti-stabilized ferritic stainless steel containing 11 mass pct Cr. They reported that the inclusions in the steel melt equilibrated with the basic slags ($\text{basicity} = [\text{CaO} + \text{MgO}]/[\text{SiO}_2 + \text{Al}_2\text{O}_3] > 1.7$) were located in the spinel+liquid multiphase region, while those in equilibrium with the less basic slags ($\text{basicity} < 1.7$) were mostly located in the fully liquid region. Kim *et al.*^[26] investigated the formation of complex oxide inclusions in Al-Ti deoxidized 304 stainless steel. They concluded that a decrease in the slag basicity was the most effective way to reduce the crystallization of the harmful CaO-TiO_2 phase in inclusions. Li *et al.*^[27] investigated the effect of $\text{CaO-MgO-SiO}_2\text{-Al}_2\text{O}_3\text{-TiO}_2\text{-CaF}_2$ slags containing different CaF_2 contents on the inclusion characteristics in a Al deoxidized Ti-stabilized 20 mass pct Cr stainless steel. They concluded that the lower the CaF_2 content in slag, the lower MgO content of inclusions in steel, which made most of the inclusions located in or close to the liquid phase field.

High basicity slags have commonly been used in Al-killed steels to reach a high cleanliness and inclusions having low melting temperature.^[28–30] Nevertheless, the effect of slag on the high TiO_x contained inclusions in Ti-containing stainless steel has been under discussion. Therefore, in the present study, the refractory-slag-metal reaction experiments were performed to investigate the

effect of the $\text{CaO-SiO}_2\text{-Al}_2\text{O}_3\text{-MgO}$ slag on the evolution of oxide inclusions in Ti-containing 24 mass pct Cr stainless steel.

II. METHODOLOGY

A. Experimental Procedures

The experiment was carried out using a high-frequency induction furnace, which is shown in Figure 1(a). The quartz reaction chamber was initially evacuated using a mechanical rotary pump prior to performing the experiments; the chamber was subsequently filled with a highly purified Ar-3 pct H_2 gas mixture controlled using a mass flow controller. Impurities in the Ar-3 pct H_2 gas mixture were removed by passing the gas through Drierite (W.A. Hammond Drierite Co. Ltd., Xenia, OH), silica gel, and Mg turnings at 723 K (450 °C). The 430 steel ingot (500 g) was melted in a fused MgO crucible (99.9 pct purity, 60 × 50 × 120 mm) with a graphite heater for induction heating; the heater was surrounded by insulation. The experimental temperature was 1873 K (1600 °C), which was controlled within ± 2 K (2 °C) using a B-type (Pt-30Rh/Pt-6Rh, mass pct) thermocouple and a proportional integral differential controller. After the temperature was stabilized for 30 min, 85 g FeCr alloy was added through the quartz tube (14 × 12 × 500 mm) under an Ar-3 pct H_2 atmosphere. The chemical compositions of the steel and FeCr alloy are shown in Table I.

Several steel samples were taken after the FeCr addition, and the inclusion characterization results were reported elsewhere.^[31] After 30 min of the alloy addition, sample S0 was taken from the molten steel using a quartz tube (ID = 4 mm). Thereafter, 50 g slag was added on the surface of molten steel under an Ar-3 pct H_2 atmosphere. The slag was prepared by melting reagent grades of SiO_2 , Al_2O_3 , MgO and CaO in advance in a vertical resistance tube furnace under a purified Ar atmosphere. Here, CaO was obtained from a reagent grade of CaCO_3 , which was calcined at 1273 K (1000 °C) for 12 hours. Then, steel samples were taken at predetermined times after the slag addition (S1-5 min, S2-15 min, S3-25 min) and rapidly quenched in water. Slag samples were also taken using stainless steel rods at the predetermined times (Slag 1-5 min, Slag 2-15 min, Slag 3-25 min), as shown in Figure 1 (b).

B. Analysis and Characterization

The chemical compositions of the steel and slag samples were determined using inductively coupled plasma atomic emission spectrometry (ICP-AES, ACROS, SPECTRO) and X-ray fluorescence spectroscopy (XRF, Bruker, model S4 Explorer). The oxygen and nitrogen contents were determined by using a LECO combustion analyzer. Three-dimensional observations using the electrolytic extraction method were used to observe the exact morphology and composition of inclusions in the steel samples. For this experiment, a 10 pct AA solution (10 pct acetylacetone,

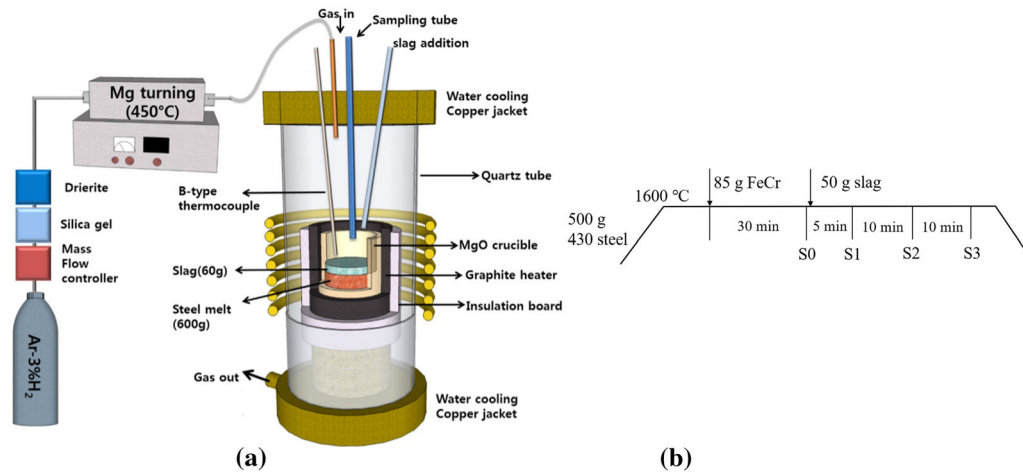


Fig. 1—Schematic diagram of the experimental apparatus (a) and schematic illustration of the sampling time (b).

Table I. Chemical Compositions of Steel and FeCr Alloy Used in the Present Study (Mass Pct)

Elements	C	Si	Mn	Cr _x	Ti	Al	N	S	O
430 Steel	0.004	0.12	0.15	16.5	0.22	0.012	0.006	0.003	0.01
FeCr	0.03	0.41	0.25	71.8	0.12	0.05	0.021	0.002	0.078

1 pct tetramethylammonium chloride, and methanol) was used as the electrolyte, and a 750 mA current was applied for 3 h. The extracted inclusions were filtered out by using a vacuum pump and laid on a membrane filter with a pore size of 0.1 μm . Once completely dried, the filter was coated with platinum. Next, the inclusions on the filter were investigated using field emission scanning electron microscopy analysis (FESEM; TESCAN model MIRA 3) with an energy-dispersive X-ray spectroscope (EDS). Besides, the characterization of inclusions in two-dimensional, *i.e.*, number density, size and composition, in the steel samples was performed using the automated inclusion analysis system. The following settings were applied: accelerating voltage 20 KV, magnification 500 times and a 1 μm limit diameter for inclusion detection in a 10 mm² area.

III. RESULTS AND DISCUSSION

A. Characterization of Inclusions

SEM images of typical inclusions found in the samples before and after the slag addition are shown in Figure 2. To get stable TiO_x and $\text{TiO}_x\text{-CrO}_x$ based inclusions, FeCr alloys were added into the Ti-containing steels. The inclusion characteristics can be found from previous work,^[31] where Ti_2O_3 and Cr_2O_3 were chosen to represent the Ti oxide and Cr oxide in inclusions. Before the slag addition, the main inclusions were $\text{Ti}_2\text{O}_3\text{-Cr}_2\text{O}_3$ based systems containing a small amount of Al_2O_3 content. It should be pointed out that the $\text{Ti}_2\text{O}_3\text{-Cr}_2\text{O}_3$ based inclusions have rarely been reported before. They can

further be divided into two groups based on their morphologies and compositions: irregular shapes with lower Cr_2O_3 contents (Figure 2(a)) and globular shapes with higher Cr_2O_3 contents (Figure 2(b)). In addition, a small number of spherical $\text{Ti}_2\text{O}_3\text{-Cr}_2\text{O}_3\text{-SiO}_2$ inclusions (Figure 2(c)) were also observed.

In sample S1 taken after 5 min of the slag addition, the number of inclusions significantly increased due to the slag-steel reactions. A relatively larger amount of inclusions were located together on the film filters, as shown in Figure 2(d). The original $\text{Ti}_2\text{O}_3\text{-Cr}_2\text{O}_3$ based inclusions with different morphologies (Figure 2(e) and (f)) still existed. Besides, spherical (Figure 2(g)) shape $\text{Ti}_2\text{O}_3\text{-Cr}_2\text{O}_3\text{-Al}_2\text{O}_3$ inclusions were observed, which had higher Al_2O_3 contents compared to the $\text{Ti}_2\text{O}_3\text{-Cr}_2\text{O}_3$ based inclusions. The corresponding elemental mappings of these $\text{Ti}_2\text{O}_3\text{-Cr}_2\text{O}_3\text{-Al}_2\text{O}_3$ inclusions are shown in Figure 3(a).

It is of interest to note that dual-phase $\text{Ti}_2\text{O}_3\text{-Cr}_2\text{O}_3\text{-SiO}_2$ inclusions were commonly observed in this sample, where the Al_2O_3 content was less than 5 mass pct. They consisted of a dark grey phase having higher Si contents and a light grey phase with lower Si contents (Figures 2(h) and (i)). In addition, some dark phases contained Ti_2O_3 , Cr_2O_3 , SiO_2 and Al_2O_3 four components (Figure 2(j)). The elemental mappings of the typical dual-phase $\text{Ti}_2\text{O}_3\text{-Cr}_2\text{O}_3\text{-SiO}_2$ inclusions are shown in Figures 3(b) through (d). Homogenous spherical $\text{Ti}_2\text{O}_3\text{-Cr}_2\text{O}_3\text{-SiO}_2$ inclusions were also found (Figure 2(k)), the elemental mappings are shown in Figure 3(e). Moreover, spherical complex $\text{Ti}_2\text{O}_3\text{-Cr}_2\text{O}_3\text{-SiO}_2\text{-Al}_2\text{O}_3$ inclusions were observed (Figure 2(l)). In addition, they were found in all the following samples.

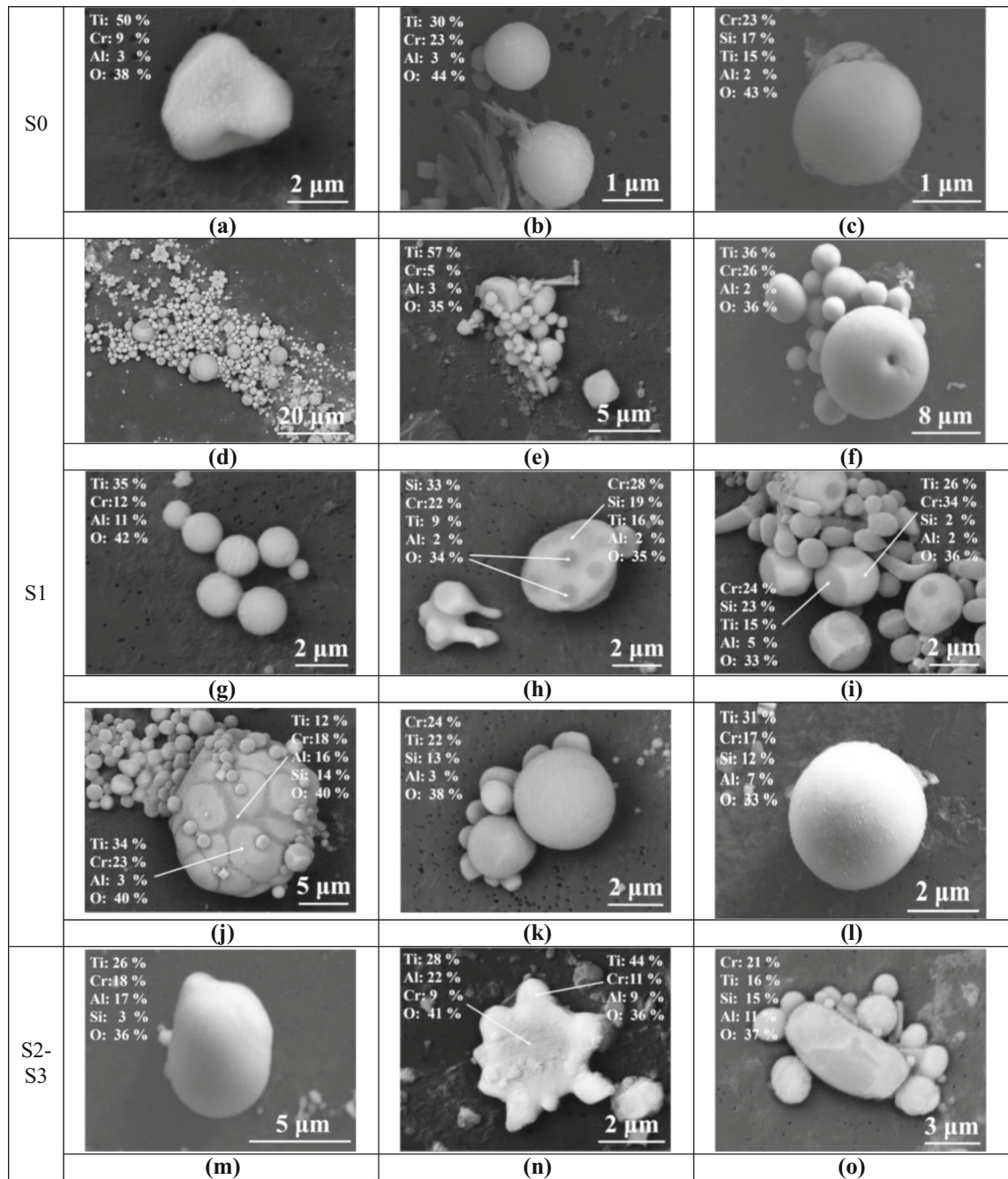


Fig.2—Morphologies and compositions of typical inclusions in different samples: (a), (b) and (c) in S0, (d) through (l) in S1, (m) through (o) in S2 and S3.

In sample S2 taken after 15 min of the slag addition, the number of inclusions significantly reduced, which is discussed in detail in Figure 5 later. Moreover, most irregular shaped Ti_2O_3 - Cr_2O_3 based inclusions disappeared and were transformed into spherical (Figure 2(m)) and polygonal (Figure 2(n)) Ti_2O_3 - Cr_2O_3 - Al_2O_3 inclusions. Specifically, the polygonal type consisted of a homogeneous one and a heterogeneous one containing higher Al_2O_3 contents in the center. Their mappings results are shown in Figures 3(f) and (g). In addition, spherical complex Ti_2O_3 - Cr_2O_3 - SiO_2 - Al_2O_3 inclusions (Figure 2(o)) were more commonly observed

than Ti_2O_3 - Cr_2O_3 - SiO_2 inclusions. It should be noted that the Ti_2O_3 - Cr_2O_3 - SiO_2 - Al_2O_3 inclusions started to form in sample S1 (5 min) and that the Al_2O_3 contents in these inclusions obviously increased with time. In the final sample S3 taken after 25 min of the slag addition, the types of inclusions were similar to those found in sample S2, but with some composition changes.

To investigate the evolution of inclusions, the compositions of inclusions in different samples were projected onto the CrO_x - Ti_2O_3 - Al_2O_3 and CrO_x - Ti_2O_3 - SiO_2 ternary phase diagrams, as shown in Figure 4. The phase diagrams were calculated with the aid of FactSage 7.1

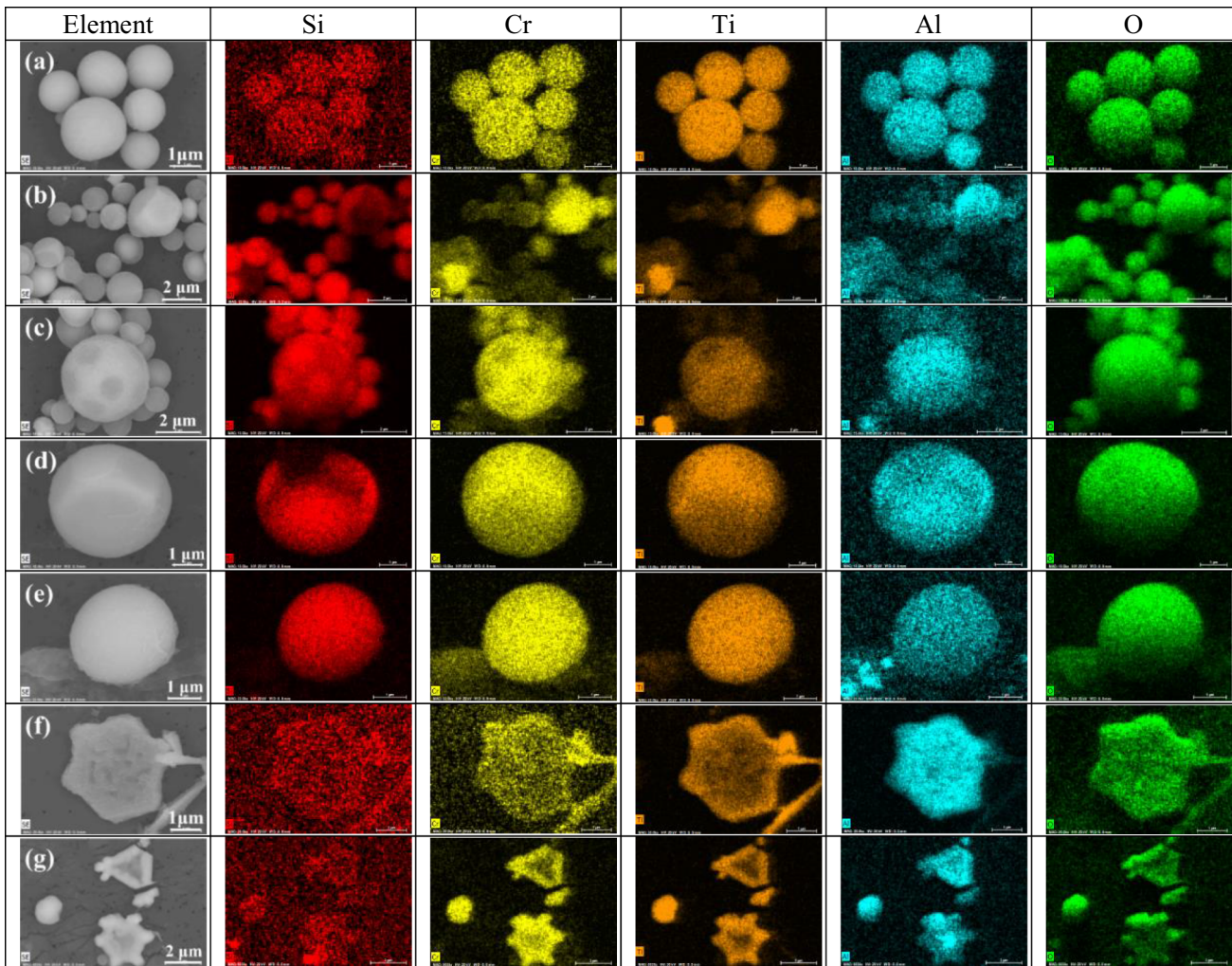


Fig. 3—Element mappings of typical inclusions (a) spherical $\text{Ti}_2\text{O}_3\text{-Cr}_2\text{O}_3\text{-Al}_2\text{O}_3$ inclusions, (b) through (d) multiphase $\text{Ti}_2\text{O}_3\text{-Cr}_2\text{O}_3\text{-SiO}_2$ inclusions, (e) homogeneous $\text{Ti}_2\text{O}_3\text{-Cr}_2\text{O}_3\text{-SiO}_2$ inclusions, (f) and (g) polygonal $\text{Ti}_2\text{O}_3\text{-Cr}_2\text{O}_3\text{-Al}_2\text{O}_3$ inclusions.

software using the FactPS and FToxid databases at 1873 K (1600 °C) and $p(\text{O}_2) = 10^{-15}$ atm, which was calculated based on the measured oxygen content. The details of the calculation to determine the oxygen partial pressure in the present system is given elsewhere.^[31] It can be seen from Figure 4(a) that the main compositions of inclusions are concentrated in the single liquid and $\text{Ti}_2\text{O}_3 + \text{liquid}$ regions before the slag addition. After 5 min of the slag addition (S1), the number of inclusions significantly increases, as shown in Figure 4(b). The majority of inclusions are located in the single liquid region. The Ti_2O_3 contents slightly decrease while the Al_2O_3 contents in inclusions are higher than those in sample S0 (Figure 4(a)). In sample S2 (15 min), the Al_2O_3 contents in inclusions continue to increase and there are very few inclusions in the $\text{Ti}_2\text{O}_3 + \text{liquid}$ region (Figure 4(c)). The tendency is more obvious as most of the inclusions move towards the $\text{Al}_2\text{O}_3 + \text{liquid}$ region in sample S3 (Figure 4(d)). Therefore, the slag addition has a great effect on the transformations of inclusions.

The composition distributions of homogeneous and multiphase $\text{Ti}_2\text{O}_3\text{-Cr}_2\text{O}_3\text{-SiO}_2$ inclusions in all four samples are presented in Figure 4(e). As can be seen, most of the inclusions are located in the single liquid phase region. Also, a small number of inclusions with higher SiO_2 contents are located in the $\text{SiO}_2 + \text{liquid}$ region, which corresponds to the high SiO_2 phase in the multiphase inclusions. However, it should be noted that the automatic two-dimensional SEM analysis only resolves one point composition of each inclusion. Thus, there might be more multiphase inclusions present. In terms of the homogeneous $\text{Ti}_2\text{O}_3\text{-Cr}_2\text{O}_3\text{-SiO}_2\text{-Al}_2\text{O}_3$ inclusions (Figure 4(f)), the Al_2O_3 contents in these inclusions are first grouped with the Cr_2O_3 contents and then their compositions are projected onto the $\text{CrO}_x\text{-Ti}_2\text{O}_3\text{-SiO}_2$ ternary phase diagram. Most of the inclusions are located in the liquid area, and their composition distributions overlapped to some extent. Moreover, the $\text{Cr}_2\text{O}_3 + \text{Al}_2\text{O}_3$ contents obviously increase and the Ti_2O_3 contents decrease with time.

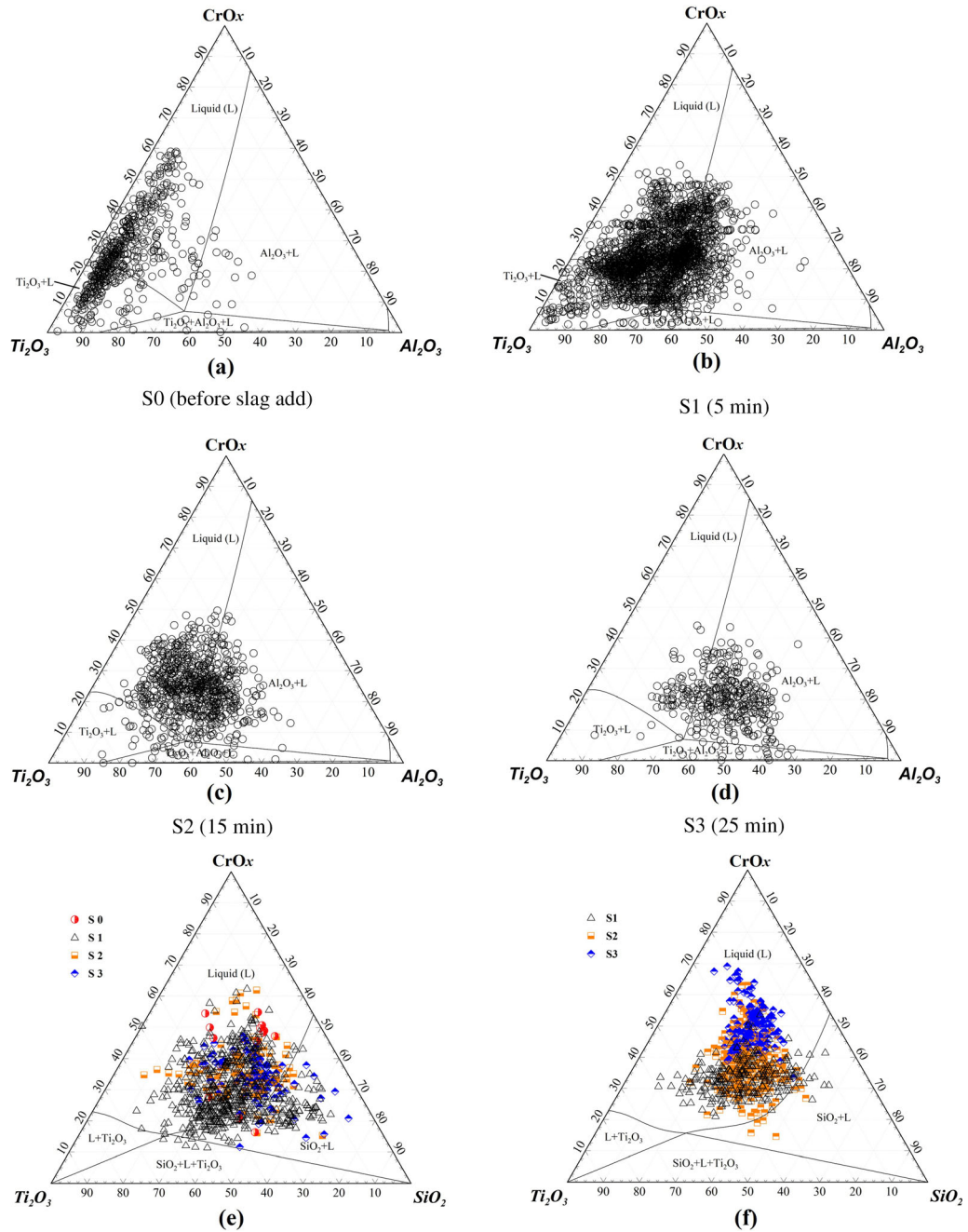


Fig. 4—Compositions of inclusions in steel samples, projected onto the 1873 K isotherm of the CrO_x - Ti_2O_3 - Al_2O_3 ternary diagram: (a) S0-0 min, (b) S1-5 min, (c) S2-15 min, (d) S3-25 min, and the CrO_x - Ti_2O_3 - SiO_2 ternary diagram: (e) Ti_2O_3 - Cr_2O_3 - SiO_2 inclusions and (f) Ti_2O_3 - Cr_2O_3 - SiO_2 - Al_2O_3 inclusions (The axis number represents mass pct).

The number density and area fraction variations of different types of inclusions show similar tendency, which are illustrated in Figure 5. Before the slag addition (S0), the major type is the Ti_2O_3 - Cr_2O_3 - Al_2O_3 system inclusions. After 5 min of the slag addition (S1), the number of this type of inclusions has increased by about 5 times. A large number of inclusions have been formed due to the slag-steel reactions. Thereafter, their number continues to decrease with time due to the inclusion floatation and absorption of inclusions by slag.

Finally, their number approximately reduces by half in sample S3 (25 min) compared to that in sample S0 before the slag addition.

The number of Ti_2O_3 - Cr_2O_3 - SiO_2 inclusions (multi-phase and homogeneous) also greatly increases in sample S1. The number density of Ti_2O_3 - Cr_2O_3 - SiO_2 inclusions is almost twice more than that of Ti_2O_3 - Cr_2O_3 - SiO_2 - Al_2O_3 inclusions. In sample S2, the reduction of the number density of Ti_2O_3 - Cr_2O_3 - SiO_2 inclusions is much greater than that of

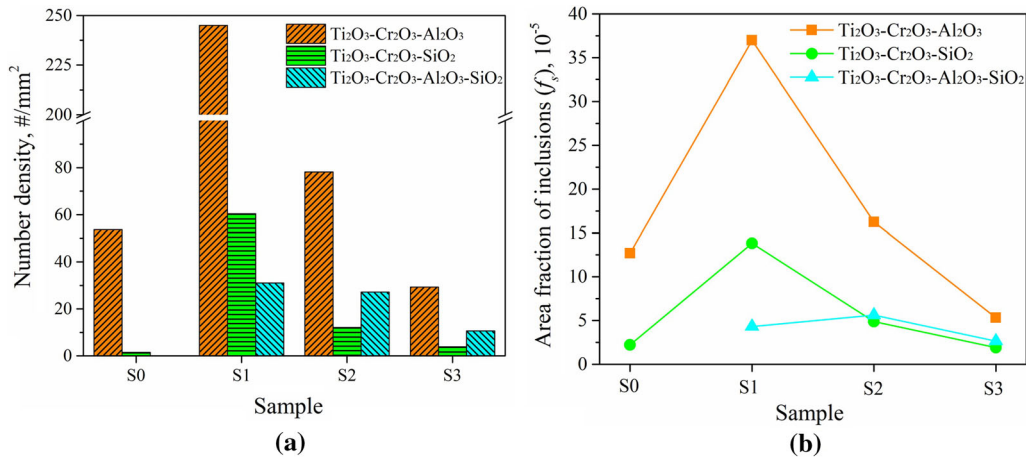


Fig. 5—Number density (a) and area fraction (b) changes of different types of inclusions.

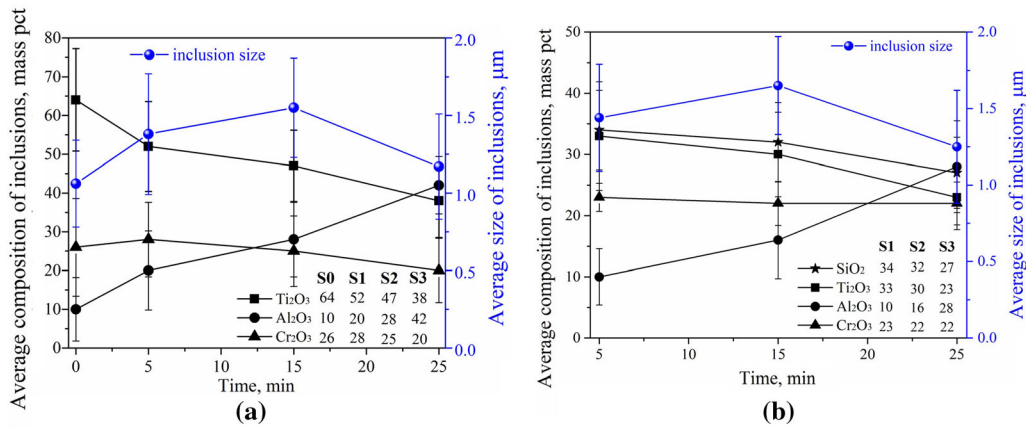


Fig. 6—Average compositions and size changes of (a) $\text{Ti}_2\text{O}_3\text{-Cr}_2\text{O}_3\text{-Al}_2\text{O}_3$ and (b) $\text{Ti}_2\text{O}_3\text{-Cr}_2\text{O}_3\text{-SiO}_2\text{-Al}_2\text{O}_3$ inclusions.

$\text{Ti}_2\text{O}_3\text{-Cr}_2\text{O}_3\text{-SiO}_2\text{-Al}_2\text{O}_3$ inclusions. This might be attributed to the fact that some $\text{Ti}_2\text{O}_3\text{-Cr}_2\text{O}_3\text{-SiO}_2$ inclusions have been transformed into $\text{Ti}_2\text{O}_3\text{-Cr}_2\text{O}_3\text{-SiO}_2\text{-Al}_2\text{O}_3$ inclusions. This tendency continues with time and the $\text{Ti}_2\text{O}_3\text{-Cr}_2\text{O}_3\text{-SiO}_2\text{-Al}_2\text{O}_3$ inclusions are more dominant in the SiO_2 containing inclusions in the final sample S3.

The effect of the slag addition on the average compositions and sizes of $\text{Ti}_2\text{O}_3\text{-Cr}_2\text{O}_3\text{-Al}_2\text{O}_3$ and $\text{Ti}_2\text{O}_3\text{-Cr}_2\text{O}_3\text{-SiO}_2\text{-Al}_2\text{O}_3$ inclusions is shown in Figure 6. The Al_2O_3 contents in $\text{Ti}_2\text{O}_3\text{-Cr}_2\text{O}_3\text{-Al}_2\text{O}_3$ inclusions significantly increase from 10 to 42 mass pct, while the Ti_2O_3 and Cr_2O_3 contents decrease after the slag additions. These results indicate that the oxides of Ti_2O_3 and Cr_2O_3 are reduced by dissolved Al. The composition change of $\text{Ti}_2\text{O}_3\text{-Cr}_2\text{O}_3\text{-SiO}_2\text{-Al}_2\text{O}_3$ inclusions shows a similar tendency to that of $\text{Ti}_2\text{O}_3\text{-Cr}_2\text{O}_3\text{-Al}_2\text{O}_3$ inclusions. The final Al_2O_3 contents in the $\text{Ti}_2\text{O}_3\text{-Cr}_2\text{O}_3\text{-SiO}_2\text{-Al}_2\text{O}_3$ inclusions reach about 30 mass pct, and the Ti_2O_3 and SiO_2 contents slightly decrease. The composition distributions of this type of inclusions move towards the $\text{Cr}_2\text{O}_3 + \text{Al}_2\text{O}_3$ corner with time (Figure 4(f)) and these are primarily due to the increase of the Al_2O_3 contents. The average sizes of

these two types of inclusions first increase and reach a peak at 15 min and then decrease. Their final sizes have similar values of approximately $1.2 (\pm 0.3) \mu\text{m}$.

B. Slag-Steel Reactions

1. Composition change of molten steel and slag

After the slag addition, it took about 3 min for the slag to be fully melted, as shown in Figure 7. The compositions of the initial premelted slag, and the slag and steel samples taken at different times are shown in Table II and Figure 8. A high basicity ($(\text{CaO})/(\text{SiO}_2) \approx 6$) MgO saturated slag was used in the present study. After the slag addition, the CaO and SiO_2 contents slightly decreased, while the Al_2O_3 content increased (but not significant) with time. It should be noted that titanium oxide generated after the slag-steel reactions and continuously increased with time, indicating the oxidation of Ti in the steel. Here, the titanium oxide is assumed to be TiO_2 for the sake of simplicity. In terms of the steel compositions, the Ti content significantly decreased while the Al content only gradually decreased with time. The Si content showed an increasing tendency with time but with a small fluctuation, which increased

greatly during the first 5 min. The total O content decreased from 62 to 26 ppm after the slag addition, which indicated that the cleanliness of the steel had been improved due to the slag refining. The changes in the slag and steel compositions were due to the slag-steel reactions.

The activities of the slag components at the initial and final compositions were calculated with an aid of FactSage 7.1 software using the FToxide database, the results are shown in Figure 9. The activity of CaO decreases with time, whereas the activities of Al₂O₃, SiO₂ and TiO₂ all increase with time. Besides, the activity of Al₂O₃ is much higher than those of SiO₂ and TiO₂. This can be explained by the fact that the TiO₂ in the slag is an acidic oxide which has a strong affinity with CaO. Thus, the activity of CaO decreases with an increased TiO₂ content. Therefore, the relative attraction between SiO₂, Al₂O₃ and CaO decreases, which further increases the SiO₂ and Al₂O₃ activity.^[32] Therefore, the activity changes of slag component not simply depend on their compositions, but also the attractive force between different components. The activity changes of the slag components have a significant influence on the Al, Ti and Si contents in the steel melts.

During the refining process of Ti-bearing stainless steel, the slag-steel reaction could lead to the loss of titanium in molten steel.^[27,33] The SiO₂ and Al₂O₃ in slag can react with Ti in molten steel according to Eqs. [1] and [4], which would cause a loss of Ti in steel.^[10,27,32,34] Moreover, considering the mass balance of the decrease of SiO₂ and the increase of TiO₂ in the slag, both reactions happened in the present study. Also, the increase of Al₂O₃ in the slag might be due to the reaction between SiO₂ in the slag and Al in the molten steel based on Eq. [7].

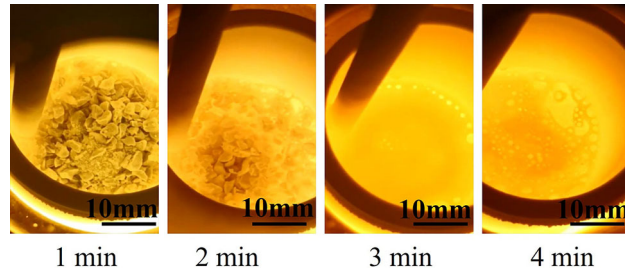
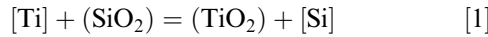


Fig. 7—Melting process of slag during the experiment.

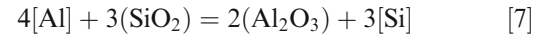
$$\log K_1 = \log \frac{a_{\text{Si}} \cdot a_{\text{TiO}_2}}{a_{\text{Ti}} \cdot a_{\text{SiO}_2}} = \log \frac{f_{\text{Si}} \cdot [\text{Pct Si}] \cdot a_{\text{TiO}_2}}{f_{\text{Ti}} \cdot [\text{Pct Ti}] \cdot a_{\text{SiO}_2}} \quad [2]$$

$$\log \frac{[\text{Pct Ti}]}{[\text{Pct Si}]} = \log \frac{a_{\text{TiO}_2}}{a_{\text{SiO}_2}} + \log \frac{f_{\text{Si}}}{f_{\text{Ti}}} - \log K_1 \quad [3]$$



$$K_4 = \frac{a_{\text{Al}}^4 \cdot a_{\text{TiO}_2}^3}{a_{\text{Ti}}^3 \cdot a_{\text{Al}_2\text{O}_3}^2} = \frac{f_{\text{Al}}^4 \cdot [\text{Pct Al}]^4 \cdot a_{\text{TiO}_2}^3}{f_{\text{Ti}}^3 \cdot [\text{Pct Ti}]^3 \cdot a_{\text{Al}_2\text{O}_3}^2} \quad [5]$$

$$\log \frac{[\text{Pct Al}]^4}{[\text{Pct Ti}]^3} = \log \frac{a_{\text{Al}_2\text{O}_3}^2}{a_{\text{TiO}_2}^3} + \log \frac{f_{\text{Ti}}^3}{f_{\text{Al}}^4} - \log K_4 \quad [6]$$



$$\log K_7 = \frac{a_{\text{Si}}^3 \cdot a_{\text{Al}_2\text{O}_3}^2}{a_{\text{Al}}^4 \cdot a_{\text{SiO}_2}^3} = \frac{f_{\text{Si}}^3 \cdot [\text{Pct Si}]^3 \cdot a_{\text{Al}_2\text{O}_3}^2}{f_{\text{Al}}^4 \cdot [\text{Pct Al}]^4 \cdot a_{\text{SiO}_2}^3} \quad [8]$$

$$\log \frac{[\text{Pct Al}]^4}{[\text{Pct Si}]^3} = \log \frac{a_{\text{Al}_2\text{O}_3}^2}{a_{\text{SiO}_2}^3} + \log \frac{f_{\text{Si}}^3}{f_{\text{Al}}^4} - \log K_7 \quad [9]$$

where a_{TiO_2} , a_{SiO_2} and $a_{\text{Al}_2\text{O}_3}$ are the activities of TiO₂, SiO₂ and Al₂O₃ in the slag; f_{Ti} , f_{Si} and f_{Al} are the Henrian activity coefficients of Ti, Si and Al in the steel.

According to Eqs. [3], [6] and [9], the dependence of the composition ratios of steel on the activity ratios of slag in different samples can be calculated, as shown in Figure 10. Based on Eq. [3], the increase of $\log(a_{\text{TiO}_2}/a_{\text{SiO}_2})$ in the slag could cause an increase of $\log[\% \text{Ti}]/[\% \text{Si}]$ in the molten steel. This, in turn, can result in higher Ti contents and lower Si contents in the steel melt. It indicates that an increased TiO₂ activity can lead to a higher Ti content in the steel melt, which is also obtained in the following kinetics analysis. However, it should be pointed out that the increased TiO₂ activity should be obtained in the original slag before

Table II. Compositions of the Steel and Slag Samples Investigated in the Present Study

Sample	Metal				Slag, Mass Pct				
	[Ti, Pct]	[Si, Pct]	[Al, Pct]	[O, ppm]	CaO	Al ₂ O ₃	MgO	SiO ₂	TiO ₂
S0	0.13	0.20	0.01	62	53.2	31.4	6.4	9	0
S1	0.03	0.28	0.01	45	51.7	31.7	6.4	8.6	1.6
S2	0.03	0.26	0.01	34	49.9	32.7	6.9	7.8	2.7
S3	0.02	0.28	0.01	27	48.0	34.1	7.5	7.3	3.1

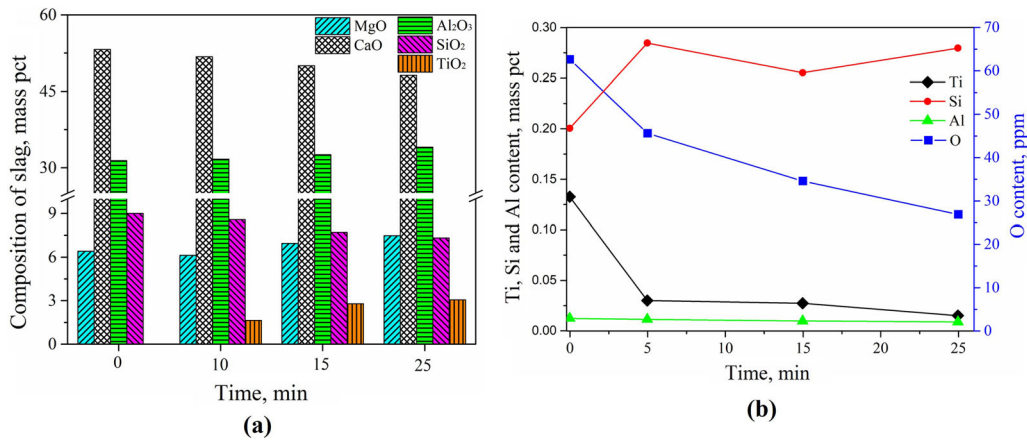


Fig. 8—Chemical compositions of the initial slag sample and slag samples after slag-steel reactions (a) and steel samples (b).

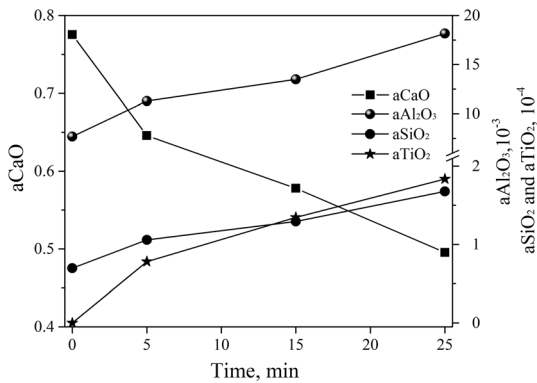


Fig. 9—The activity changes of CaO, Al₂O₃, SiO₂ and TiO₂ in the slag samples (Reference states are pure oxides at the calculation temperature, and 1 atm.).

the slag-steel reactions. The measured values of $\log[\%Ti]/[\%Si]$ decrease when the $\log(a_{TiO_2}/a_{SiO_2})$ of slag increases, which is due to the fact that the TiO₂ is formed after the slag-steel reactions in the present study (Figure 10(a)). Similarly, in the case of Eq. [6], the decrease of $\log(a_{Al_2O_3}^2/a_{TiO_2}^3)$ slag could cause a decrease of $\log([\%Al]^4/[\%Ti]^3)$ in the molten steel, but the experimental results also showed the opposite tendency (Figure 10(b)). Moreover, both the Al and Ti contents

decreased with time as shown in Figure 8(b). Therefore, the reduction of the Ti content was greater than that of Al in the molten steel, which indicated that Eq. [4] might not be the main reaction. The decrease of $\log(a_{Al_2O_3}^2/a_{SiO_2}^3)$ of slag could cause a decrease of $\log([\%Al]^4/[\%Si]^3)$ in the molten steel according to Eq. [9], where a similar tendency of the measured values of $\log([\%Al]^4/[\%Si]^3)$ was obtained as shown in Figure 10(c). Based on these discussions, the final steel composition changes depend on these coupled reactions.

C. Kinetics of Slag-Steel Reactions

The coupled-reaction model and two film theory have frequently been applied to describe the kinetics of slag-steel reactions.^[30,32,35,36] It is assumed that the concentrations of Al₂O₃, TiO₂, SiO₂ in the slag side and Al, Ti, Si and O in the steel show respective concentration gradients in the boundary film layer at the slag-steel interface, and have reached a thermodynamic equilibrium at the interface, as shown in Figure 11.

In the present study, the reactions [10], [12] and [14] were simultaneously considered to take place at the slag-steel interface. Assuming that these reactions occur rapidly during the present conditions, and local equilibrium reaches at the slag-steel interface. The corresponding equilibrium constants K for each reaction can be calculated.^[37–39] To simplify the computation, AlO_{1.5} is used. Apparent equilibrium constant B_i can be expressed by Eq. [16].

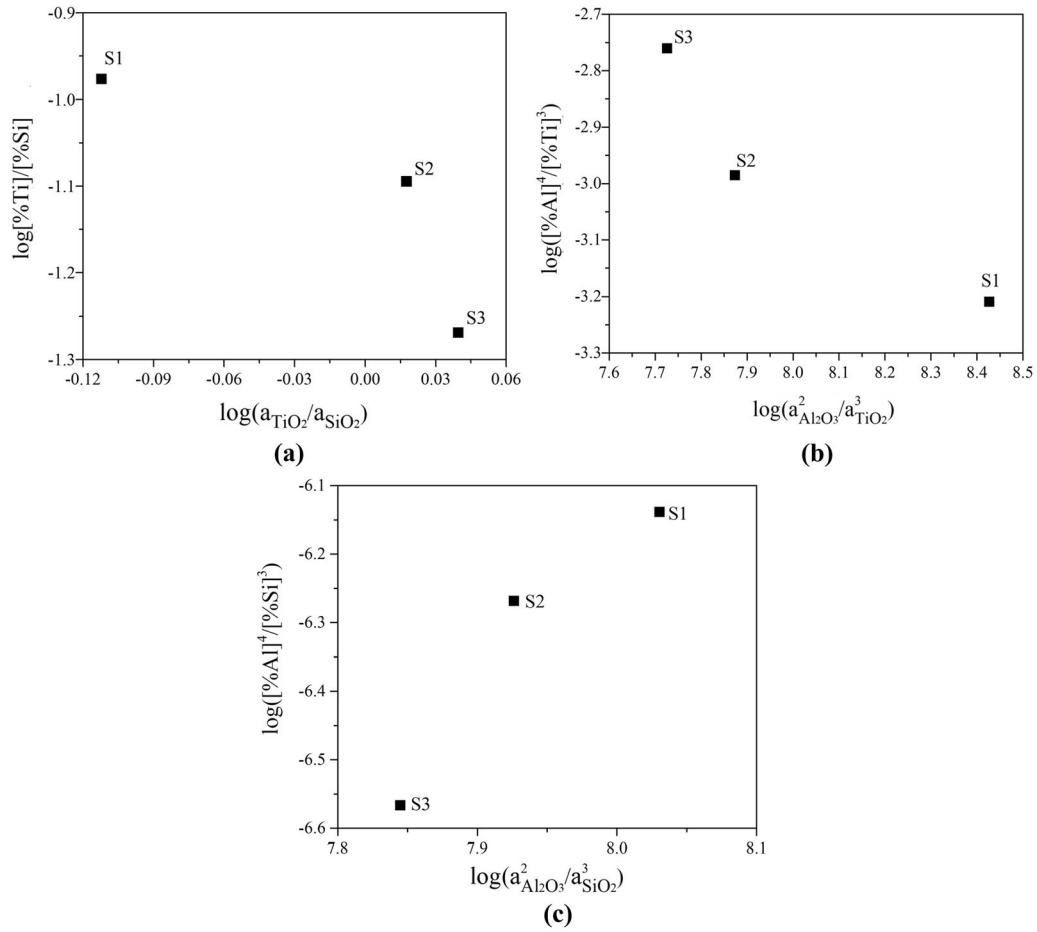


Fig. 10—Dependence of the composition ratios of steel on the activity ratios of slag (a) $\log(a_{\text{TiO}_2}/a_{\text{SiO}_2})$ to $\log[\% \text{Ti}]/[\% \text{Si}]$, (b) $\log(a_{\text{Al}_2\text{O}_3}^2/a_{\text{TiO}_2}^3)$ to $\log([\% \text{Al}]^4/[\% \text{Ti}]^3)$ and (c) $\log(a_{\text{Al}_2\text{O}_3}^2/a_{\text{SiO}_2}^3)$ to $\log([\% \text{Al}]^4/[\% \text{Si}]^3)$.

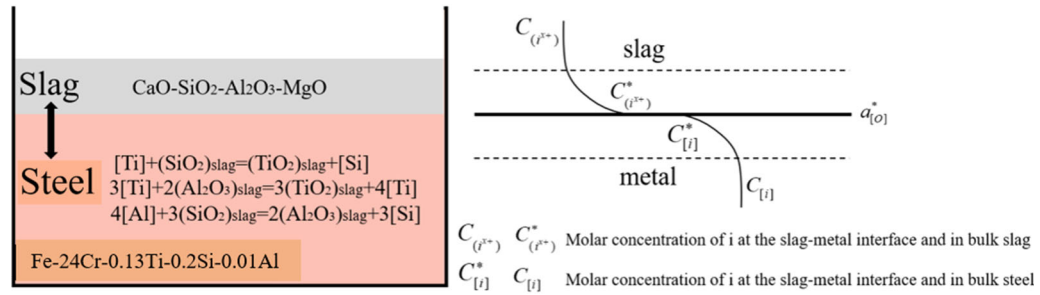
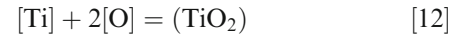
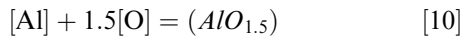
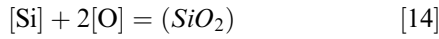


Fig. 11—The schematic diagram for the reaction between slag and steel.



$$\begin{aligned} \log K_{10} &= \lg \frac{a_{\text{AlO}_{1.5}}^*}{a_{\text{Al}}^* \cdot a_{\text{O}}^{*1.5}} = \lg \frac{\gamma_{\text{AlO}_{1.5}} x_{\text{AlO}_{1.5}}^*}{f_{\text{Al}} \cdot [\% \text{Al}]^* \cdot f_{\text{O}}^{1.5} \cdot [\% \text{O}]^{*1.5}} \\ &= \frac{32000}{T} - 10.29 \end{aligned} \quad [11]$$

$$\begin{aligned} \log K_{12} &= \lg \frac{a_{\text{TiO}_2}^*}{a_{\text{Ti}}^* \cdot a_{\text{O}}^{*2}} = \lg \frac{\gamma_{\text{TiO}_2} x_{\text{TiO}_2}^*}{f_{\text{Ti}} \cdot [\% \text{Ti}]^* \cdot f_{\text{O}}^2 \cdot [\% \text{O}]^{*2}} \\ &= \frac{34458}{T} - 11.96 \end{aligned} \quad [13]$$



$$\begin{aligned} \log K_{14} &= \lg \frac{a_{\text{SiO}_2}^*}{a_{\text{Si}}^* \cdot a_{\text{O}}^{*2}} = \lg \frac{\gamma_{\text{SiO}_2} \chi_{\text{SiO}_2}^*}{f_{\text{Si}} \cdot [\% \text{Si}]^* \cdot f_{\text{O}}^2 \cdot [\% \text{O}]^{*2}} \\ &= \frac{24600}{T} - 8.4 \end{aligned} \quad [15]$$

$$B_i = \frac{(\% M_i \text{O}_n)^*}{[\% M]^* \cdot a_{\text{O}}^{*n}} = \frac{f_i \cdot K_i \cdot M_{M_i \text{O}_n} \cdot \sum \left(\frac{(\% M_i \text{O}_n)}{M_{M_i \text{O}_n}} \right)}{\gamma M_i \text{O}_n} \quad [16]$$

$$\log f_i = \sum (e_i^j [\% j] + r_i^j [\% j]^2) \quad [17]$$

where a_i is the activity of element i in the metal, f_i is the Henrian activity coefficient of element i referred to 1 pct standard state with mass percentage [% i] as the concentration unit, which can be calculated by the classical Wagner formulation [17], using the first- (e_i^j) and second-order (r_i^j) interaction parameters, which are listed in Table III. $M_{M_i \text{O}_n}$ and $\gamma M_i \text{O}_n$ are the molecular weight and activity coefficient of $M_i \text{O}_n$ in slag. [% M] and $(\% M_i \text{O}_n)$ are the mass concentration of element i in steel and $M_i \text{O}_n$ in slag.

Because the rates of the chemical reactions involving the respective component at the slag-steel interface are extremely large. Thus, mass transfer is the rate-determining step, which can be controlled by the mass transfer of metal in the steel side and slag component in the slag side. Therefore, the respective mass transfer resistance of metal (R_{M_i}) and slag component ($R_{M_i \text{O}_n}$) can be expressed by Eq. [18], which can express the controlling step in the reactions. During the transfer of component i from molten steel to slag, the flux density should be constant, this can be expressed by Eq. [19]. The modified mass transfer coefficients can be illustrated by Eqs. [20] and [21]. Therefore, the flux density of Al, Ti, Si and O can be derived by combing Eqs. [22] through [25].

$$\frac{1}{k_i} = R_{M_i} + R_{M_i \text{O}_n} = \frac{1}{\rho_m \cdot k_{M_i, m}} + \frac{M_{M_i \text{O}_n}}{B_i \cdot M_i \cdot \rho_s \cdot a_{\text{O}}^{*n} \cdot k_{M_i \text{O}_n, s}} \quad [18]$$

$$\begin{aligned} J_i &= F_i \cdot \left([\% M]^b - [\% M]^* \right) = J_{M_i \text{O}_n} \\ &= F_{M_i \text{O}_n} \cdot \left((\% M_i \text{O}_n)^* - (\% M_i \text{O}_n)^b \right) \end{aligned} \quad [19]$$

$$F_i = \frac{k_{M_i, m} \rho_m}{100 M_i} \quad [20]$$

$$F_{M_i \text{O}_n} = \frac{k_{i, s} \rho_s}{100 M_{M_i \text{O}_n}} \quad [21]$$

$$J_{\text{Al}} = F_{\text{Al}} \left([\% \text{Al}]^b - \frac{\frac{F_{\text{Al}}}{F_{\text{AlO}_{1.5}}} [\% \text{Al}]^b + (\% \text{AlO}_{1.5})^b}{\frac{F_{\text{Al}}}{F_{\text{AlO}_{1.5}}} + B_{\text{Al}} a_{\text{O}}^{*1.5}} \right) \quad [22]$$

$$J_{\text{Ti}} = F_{\text{Ti}} \left([\% \text{Ti}]^b - \frac{\frac{F_{\text{Ti}}}{F_{\text{TiO}_2}} [\% \text{Ti}]^b + (\% \text{TiO}_2)^b}{\frac{F_{\text{Ti}}}{F_{\text{TiO}_2}} + B_{\text{Ti}} a_{\text{O}}^{*2}} \right) \quad [23]$$

$$J_{\text{Si}} = F_{\text{Si}} \left([\% \text{Si}]^b - \frac{\frac{F_{\text{Si}}}{F_{\text{SiO}_2}} [\% \text{Si}]^b + (\% \text{SiO}_2)^b}{\frac{F_{\text{Si}}}{F_{\text{SiO}_2}} + B_{\text{Si}} a_{\text{O}}^{*2}} \right) \quad [24]$$

$$J_{\text{O}} = \left([\% \text{O}]^b - [\% \text{O}]^* \right) = F_{\text{O}} \left([\% \text{O}]^b - \frac{a_{\text{O}}^*}{f_{\text{O}}} \right) \quad [25]$$

where J_i , F_i , and $F_{M_i \text{O}_n}$ stand for the is the molar flux density ($\text{mol/m}^{-2}\text{s}^{-1}$), modified mass transfer coefficients of metal and slag (m/s), respectively. Superscript ‘*’ and ‘b’ represent the slag-steel interface and bulk phase, respectively. ρ_m and ρ_s are the density of steel and slag (kg/m^{-3}), $k_{M_i, m}$ and $k_{M_i \text{O}_n, s}$ are the mass

Table III. Interaction Parameters Used in the Present Study^[10,36,40]

$e_i^j(i_i^j)$	Cr	Si	Mn	Al	Ti	N	O
O	- 0.032	- 0.066	- 0.037	- 1.17 (- 0.01)	- 0.54 (0.039)	0.043	- 0.17
Ti	0.055	- 0.025	- 0.043	0.024	0.042 (- 0.001)	- 2.04	- 1.8
Al	0.03	0.056	0.035	0.043	0.016	0.033	- 1.98 (39.82)
Si	- 0.021	0.1	- 0.007	0.058	- 0.013	0.11	- 0.12

transfer coefficients of element i and $M_i O_n$ in slag (m/s), and M_i is molecular weight of element i in steel.

The oxygen activity a_O^* at the slag-steel interface can be determined by Eq. [26]. Then, the concentrations of each element in the metal as a function of time can be calculated by Eq. [27] when the calculated a_O^* value is 2.6 ppm. The parameters used in the calculations can be found in Table IV.

$$1.5J_{Al} + 2J_{Ti} + 2J_{Si} - J_O = 0 \quad [26]$$

$$-\frac{d[\%i]}{dt} = k_{i,m} \cdot \frac{A}{V_m} ([\%i] - [\%i]^*) \quad [27]$$

Figure 12(a) shows the measured and calculated results of the concentrations of Ti, Si and Al in the steel as a function of time. It can be seen that the Si and Ti contents change more drastically during the first 5 min than during a later stage. Moreover, the calculated results of the contents of Al, Si, and Ti in the molten steel show relatively good agreement with the experimental results. Based on Eq. [18], the mass transfer resistance of the respective components on the slag side can be obtained. The calculated values for mass transfer resistances of Al_2O_3 , TiO_2 and SiO_2 are 0.23, 44 and 2.3×10^4 m²s/kg, respectively. The mass transfer resistance in molten steel is 0.71 m²s/kg. Therefore, the rate-determining step of the oxidation of Ti in the steel

and the reduction of SiO_2 in the slag are the mass transfer on the slag side. Thus, the Ti content change can be expressed by Eq. [28].

$$\frac{d[\%Ti]}{dt} = k_{Ti,m} \cdot \frac{A}{V_m} ((TiO_2) - (TiO_2)^*) \quad [28]$$

It is indicated that the Ti content change depends on the difference between the TiO_2 content in the slag and the TiO_2^* value at the slag-steel interface. According to a previous work,^[32] an increased TiO_2 content in slag can prevent a loss of titanium by the reaction of dissolved Ti in steel with alumina and silica in slag. Therefore, different TiO_2 contents in the original slag were considered, and the corresponding oxygen activity (a_O^*) values were calculated by Eq. [26]. It should be pointed out that this calculation was simply performed by increasing the TiO_2 content while keeping the proportion of other slag components unchanged. As a result, the Ti content change can be calculated by Eq. [27] when an a_O^* value is obtained. The calculated results are shown in Figure 12(b). As can clearly be seen that an increased TiO_2 content in the original slag results in a less decreased Ti content in the melt. This can be explained by the fact that a higher TiO_2 content in the slag can suppress reactions [1] and [4] to the right. From another point of view, the activities of SiO_2 and Al_2O_3 decrease with an increased TiO_2 content. Thus, reactions [1] and [4] become weakened due to the lower activities of SiO_2 and Al_2O_3 on the left side of the

Table IV. The Values of the Parameters Used in the Present Study

Parameter	Value	Parameter	Value
Mass transfer coefficient of Al, Si, Ti and O in steel	2×10^{-4} m/s ^[30]	Density of steel, ρ_{steel}	7000 kg/m ⁻³ ^[41]
Mass transfer coefficient of Al_2O_3 , TiO_2 in slag	1×10^{-5} m/s ^[30]	Density of slag, ρ_{slag}	3000 kg/m ⁻³ ^[41]
Mass transfer coefficient of SiO_2 in slag	2×10^{-6} m/s ^[30]	Weight of steel, W_{steel}	500 g
Reaction area between the steel and slag, A	$\pi \cdot (0.025)^2$ m ²	Weight of slag, W_{slag}	50 g

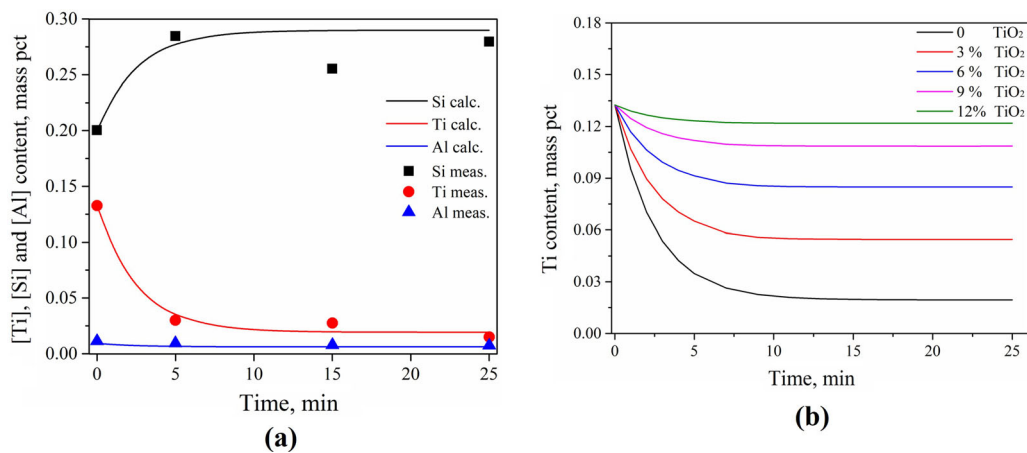


Fig. 12—Measured changes of Ti, Si and Al contents in steel melt compared with those calculated values (a) and calculated Ti contents as a function of the TiO_2 content in slag (b).

reactions. Therefore, TiO_x or complex inclusions containing TiO_x due to the reactions between Ti and SiO_2 and Al_2O_3 will be reduced. It was reported that there was an optimum TiO_2 content of about 8 mass pct due to the different combining affinity between TiO_2 and other components.^[32] However, because this kind of experimental work was not carried out in the present study, future work needs to investigate the optimum slag composition to get a low Ti loss in the steel melt.

D. Thermodynamic Calculations of Inclusion Formations

The effect of the activity of alumina in the slag on the mole fraction of alumina in the inclusions is shown in Figure 13. The mole fraction of Al_2O_3 in both $\text{Ti}_2\text{O}_3\text{-Cr}_2\text{O}_3\text{-Al}_2\text{O}_3$ and $\text{Ti}_2\text{O}_3\text{-Cr}_2\text{O}_3\text{-SiO}_2\text{-Al}_2\text{O}_3$ inclusions ($\log X_{\text{Al}_2\text{O}_3}$) increases linearly with an increased activity of Al_2O_3 ($\log a_{\text{Al}_2\text{O}_3}$) in the slag. However, it is of interest to note that the slopes of the lines are 1.4 ($r^2 = 0.99$) and 2.1 ($r^2 = 0.98$) in the $\text{Ti}_2\text{O}_3\text{-Cr}_2\text{O}_3\text{-Al}_2\text{O}_3$ and $\text{Ti}_2\text{O}_3\text{-Cr}_2\text{O}_3\text{-SiO}_2\text{-Al}_2\text{O}_3$ inclusions, respectively. This indicates that the stability of Al_2O_3 in the inclusions could significantly be affected by the reactions between slags and steel melts. Moreover, the average content changes of Al_2O_3 in both types of inclusions during the same period are nearly the same (as shown in Figure 6), while the presence of SiO_2 has a larger effect on the activity coefficient of alumina in the inclusions.

After the slag addition, the Ti_2O_3 and Cr_2O_3 contents decreased in the $\text{Ti}_2\text{O}_3\text{-Cr}_2\text{O}_3\text{-Al}_2\text{O}_3$ inclusions. This might be due to the fact that they were reduced by dissolved Al in the steel melts based on Eqs. [29] and [31].^[39,40,42] Thus, the composition of inclusions can be deduced as a function of the activities of Al, Ti, Cr and O as given in Eq. [33] and [34].

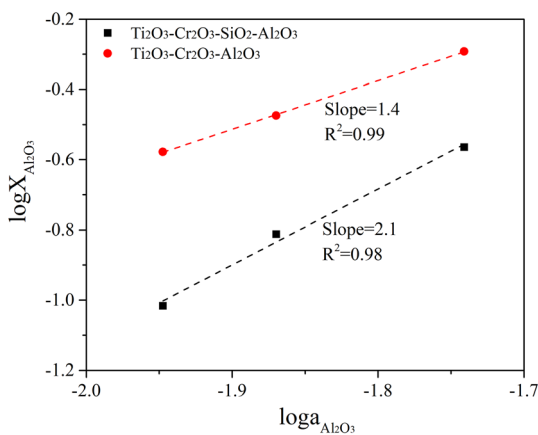
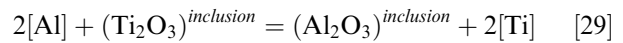
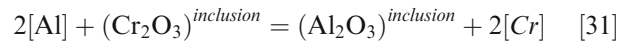


Fig. 13—Relationship between the activity of Al_2O_3 in the slag and mole fraction of Al_2O_3 in the inclusions at 1873 K (1600 °C).



$$\log K_{29} = \lg \frac{a_{\text{Ti}}^2 \cdot a_{\text{Al}_2\text{O}_3}}{a_{\text{Al}}^2 \cdot a_{\text{Ti}_2\text{O}_3}} = \frac{870}{T} - 1.44 \quad [30]$$



$$\log K_{31} = \lg \frac{a_{\text{Cr}}^2 \cdot a_{\text{Al}_2\text{O}_3}}{a_{\text{Al}}^2 \cdot a_{\text{Cr}_2\text{O}_3}} = \frac{9100}{T} + 4.48 \quad [32]$$

$$\log \frac{X_{\text{Al}_2\text{O}_3}}{X_{\text{Ti}_2\text{O}_3}} = \log \frac{a_{\text{Al}}^2}{a_{\text{Ti}}^2} - \log \frac{\gamma_{\text{Al}_2\text{O}_3}}{\gamma_{\text{Ti}_2\text{O}_3}} + \log K \quad [33]$$

$$\log \frac{X_{\text{Al}_2\text{O}_3}}{X_{\text{Ti}_2\text{O}_3} \cdot X_{\text{Cr}_2\text{O}_3}} = \log \frac{a_{\text{Al}}^2}{a_{\text{Ti}}^2 \cdot a_{\text{Cr}}^2 \cdot a_{\text{O}}^3} - \log \frac{\gamma_{\text{Al}_2\text{O}_3}}{\gamma_{\text{Ti}_2\text{O}_3} \cdot \gamma_{\text{Cr}_2\text{O}_3}} + \log K \quad [34]$$

where a_i denotes the activity of component i in steel, X_{MO} and γ_{MO} are the mole fraction and the activity coefficient of MO in the inclusions.

Therefore, it can be expected that on a logarithmic scale the mole ratios of the inclusion components are in direct proportion to the logarithmic activity ratios of Al, Ti, Cr and O in the steel melts with a slope of unity, by assuming that the activity coefficient ratio $\gamma_{\text{Al}_2\text{O}_3}/\gamma_{\text{Ti}_2\text{O}_3}$ and $\gamma_{\text{Al}_2\text{O}_3}/(\gamma_{\text{Ti}_2\text{O}_3} \cdot \gamma_{\text{Cr}_2\text{O}_3})$ in Eqs. [33] and [34] would not be significantly affected by the compositions at a fixed temperature. Their relationships are given in Figure 14. The $\log(X_{\text{Al}_2\text{O}_3}/X_{\text{Ti}_2\text{O}_3})$ and $\log[X_{\text{Al}_2\text{O}_3}/(X_{\text{Ti}_2\text{O}_3} \cdot X_{\text{Cr}_2\text{O}_3})]$ values of the inclusions increase linearly by increasing $\log(a_{\text{Al}}^2/a_{\text{Ti}}^2)$ and $\log[a_{\text{Al}}^2/(a_{\text{Ti}}^2 \cdot a_{\text{Cr}}^2 \cdot a_{\text{O}}^3)]$ values, respectively. However, it is of interest that the slope of the line for Eq. [33] is about 0.81 ($R^2=0.88$), which is smaller than the expected value of unity. Whereas the slope of the line for Eq. [34] is 1.04 ($R^2=0.99$), which is very close to unity as expected. This difference means that both Ti_2O_3 and Cr_2O_3 in the inclusions are simultaneously reduced by dissolved Al, which is in good agreement with the experimental results. The transformation tendency of the $\text{Ti}_2\text{O}_3\text{-Cr}_2\text{O}_3\text{-Al}_2\text{O}_3$ inclusions can be predicted from the thermodynamics of Al, Ti, Cr and O in the steel melts.^[10,25,43]

In terms of the SiO_2 -containing inclusions, the typical multiphase and homogeneous inclusions formed after the slag additions have been mentioned in Figure 2. These inclusions were spherical in shape but with varied Si-Ti-Cr contents. Figure 15 shows possible evolutions of these SiO_2 -containing inclusions after the slag additions. The dissolved Si content increased in the melt after the slag additions, which originated from the

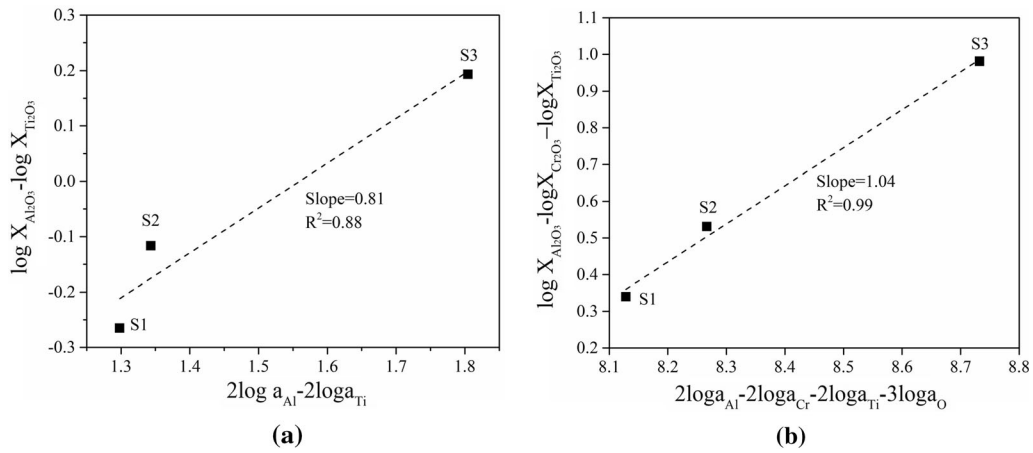


Fig. 14—Composition of $\text{Ti}_2\text{O}_3\text{-Cr}_2\text{O}_3\text{-Al}_2\text{O}_3$ inclusions (a) $\log(X_{\text{Al}_2\text{O}_3}/X_{\text{Ti}_2\text{O}_3})$ as a function of $\log(a_{\text{Al}}^2/a_{\text{Ti}}^2)$ and (b) $\log(X_{\text{Al}_2\text{O}_3}/X_{\text{Ti}_2\text{O}_3} \cdot X_{\text{Cr}_2\text{O}_3})$ as a function of $\log(a_{\text{Al}}^2/a_{\text{Ti}}^2 \cdot a_{\text{Cr}}^2 \cdot a_{\text{O}}^3)$ in steel melts at 1873 K (1600 °C).

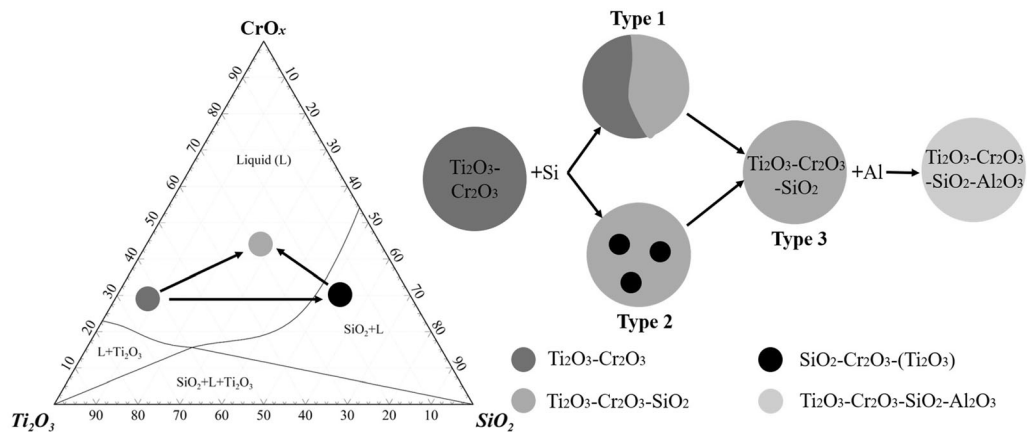
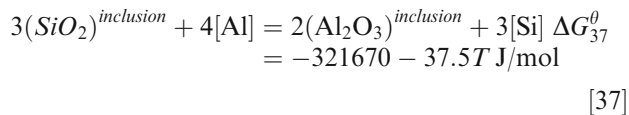
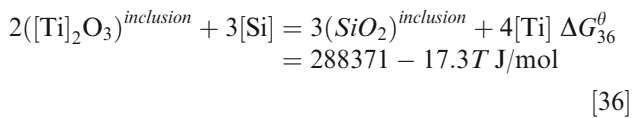
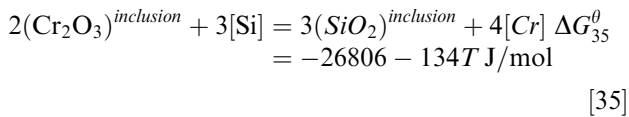


Fig. 15—Schematic illustration of the formation mechanism of the SiO_2 contained inclusions. (The axis number represents mass pct).

reduction products of the slag-steel reactions as discussed before. They reacted with the $\text{Ti}_2\text{O}_3\text{-Cr}_2\text{O}_3$ inclusions to form a $\text{Ti}_2\text{O}_3\text{-Cr}_2\text{O}_3\text{-SiO}_2$ phase, resulting in the formation of multiphase inclusions. The oxide inclusions transformed by gaining SiO_2 and losing Ti_2O_3 , Cr_2O_3 or both can be expressed by Eqs. [35] and [36]. In addition, the drop in the Ti content was higher than the Cr content in the inclusions, which suggested that Si reduced Ti_2O_3 more severely than Cr_2O_3 .

In terms of the multiphase inclusions, they can be divided into two groups: type 1 containing $\text{Ti}_2\text{O}_3\text{-Cr}_2\text{O}_3$ and $\text{Ti}_2\text{O}_3\text{-Cr}_2\text{O}_3\text{-SiO}_2$ two different phases and type 2 containing a $\text{Ti}_2\text{O}_3\text{-Cr}_2\text{O}_3\text{-SiO}_2$ phase and a $\text{SiO}_2\text{-rich SiO}_2\text{-Cr}_2\text{O}_3\text{-(Ti}_2\text{O}_3)$ phase. The compositions of the $\text{Ti}_2\text{O}_3\text{-Cr}_2\text{O}_3$ and $\text{Ti}_2\text{O}_3\text{-Cr}_2\text{O}_3\text{-SiO}_2$ phases are located in the liquid phase region, while those of the SiO_2 -rich phases are located in the SiO_2 +liquid region and they have higher melting points. In type 1 inclusions, Si in the steel continually reacted with the $\text{Ti}_2\text{O}_3\text{-Cr}_2\text{O}_3$

inclusions and were then transformed into type 3 homogeneous $\text{Ti}_2\text{O}_3\text{-Cr}_2\text{O}_3\text{-SiO}_2$ inclusions. This was also applied to the $\text{Ti}_2\text{O}_3\text{-Cr}_2\text{O}_3\text{-SiO}_2$ phases in type 2 inclusions. Moreover, the SiO_2 -rich phases in type 2 inclusions were attributed to the enrichment of Si. Thereafter, the higher chemical potential of Si in the SiO_2 -rich phases may have resulted in the diffusion of Si into the low melting $\text{Ti}_2\text{O}_3\text{-Cr}_2\text{O}_3\text{-SiO}_2$ phases. Conversely, the Ti and Cr contents in the low melting phases diffused into the SiO_2 -rich phases. When the diffusion reached a certain extent, a distinct interface between the low melting phases and SiO_2 -rich phases disappeared and spherical homogeneous type 3 $\text{Ti}_2\text{O}_3\text{-Cr}_2\text{O}_3\text{-SiO}_2$ inclusions were formed. Further, due to the increased activity of Al_2O_3 in the slag, the Ti_2O_3 , Cr_2O_3 , and also SiO_2 contents in the inclusions were simultaneously reduced by dissolved Al in the steel melts based on the Eqs. [29], [31] and [37].^[38,40,42] Finally, some $\text{Ti}_2\text{O}_3\text{-Cr}_2\text{O}_3\text{-SiO}_2$ inclusions were transformed into spherical complex $\text{Ti}_2\text{O}_3\text{-Cr}_2\text{O}_3\text{-SiO}_2\text{-Al}_2\text{O}_3$ inclusions.



IV. CONCLUSIONS

In the present study, the equilibration between a CaO-SiO₂-Al₂O₃-MgO slag and a Ti-containing ferritic stainless steel melt was investigated at 1873 K (1600 °C) to clarify the effect of the slag composition on the modification of high Ti₂O₃-containing inclusions. Moreover, the slag-steel reaction was investigated from the viewpoint of kinetics. The following conclusions were obtained.

1. The total O content greatly decreased from 62 ppm to 26 ppm after the slag addition. High Ti₂O₃-containing inclusions were transformed to Ti₂O₃-Cr₂O₃-Al₂O₃ and Ti₂O₃-Cr₂O₃-SiO₂ two system liquid inclusions after the slag addition. The number density of inclusions reached a maximum value after 5 min of the slag addition and thereafter decreased to a lower level than that before the slag addition.
2. The mole fraction of Al₂O₃ in both Ti₂O₃-Cr₂O₃-Al₂O₃ and Ti₂O₃-Cr₂O₃-SiO₂-Al₂O₃ inclusions (log $X_{\text{Al}_2\text{O}_3}$) increases linearly with an increased activity of Al₂O₃ (log $a_{\text{Al}_2\text{O}_3}$) in the slag. The Al₂O₃ content in both inclusion types obviously increased with time. The log[$X_{\text{Al}_2\text{O}_3}/(X_{\text{Ti}_2\text{O}_3} \cdot X_{\text{Cr}_2\text{O}_3})$] values of the inclusions were expressed as a linear function of the log[$a_{\text{Al}_2\text{O}_3}^2/(a_{\text{Ti}_2\text{O}_3}^2 \cdot a_{\text{Cr}_2\text{O}_3}^2)$] values of the steel melts with a slope of unity, which was theoretically expected.
3. The slag-steel reactions have a great effect on the slag and steel compositions, where the Ti content greatly decreased and TiO₂ generated in the slag. Based on the kinetic analysis, the rate-determining step of the oxidation of Ti in the steel and the reduction of SiO₂ in the slag are the mass transfer on the slag side. The addition of some amount of TiO₂ in the slag can prevent a loss of Ti in the steel melt.

ACKNOWLEDGMENTS

Yong Wang acknowledges the financial support from the China Scholarship Council (CSC). This research was partly supported by the Korea Evaluation

Institute of Industrial Technology (KEIT, with Grant No. 20009956), funded by the Ministry of Trade, Industry & Energy (MOTIE), Korea. Also, this research was partly supported by Korea Institute for Advancement of Technology (KIAT, with Grant No. P0002019), funded by the MOTIE, Korea. Yong Wang and Wangzhong Mu would like to acknowledge the Swedish Foundation for International Cooperation in Research and Higher Education (STINT with project No. IB2020-8781) and Swedish Iron and Steel Research Office (Jernkontoret).

FUNDING

Open access funding provided by Royal Institute of Technology.

OPEN ACCESS

This article is licensed under a Creative Commons Attribution 4.0 International License, which permits use, sharing, adaptation, distribution and reproduction in any medium or format, as long as you give appropriate credit to the original author(s) and the source, provide a link to the Creative Commons licence, and indicate if changes were made. The images or other third party material in this article are included in the article's Creative Commons licence, unless indicated otherwise in a credit line to the material. If material is not included in the article's Creative Commons licence and your intended use is not permitted by statutory regulation or exceeds the permitted use, you will need to obtain permission directly from the copyright holder. To view a copy of this licence, visit <http://creativecommons.org/licenses/by/4.0/>.

REFERENCES

1. X. Yin, Y. Sun, Y. Yang, X. Bai, M. Barati, and A. Mclean: *Metall. Mater. Trans. B*, 2016, vol. 47, pp. 3274–84.
2. Y. Gao and K. Sorimachi: *ISIJ Int.*, 1993, vol. 33, pp. 291–97.
3. D. Kruger and A. Garbers-Craig: *Metall. Mater. Trans. B*, 2017, vol. 48, pp. 1514–32.
4. L. Zhang, S. Taniguchi, and K. Cai: *Metall. Mater. Trans. B*, 2000, vol. 31, pp. 253–66.
5. B.H. Yoon, K.H. Heo, J.S. Kim, and H.S. Sohn: *Ironmak. Steelmak.*, 2002, vol. 29, pp. 214–17.
6. D. Zhao, H. Li, C. Bao, and J. Yang: *ISIJ Int.*, 2015, vol. 55, pp. 2115–24.
7. G. Xu, Z. Jiang, and Y. Li: *Metall. Mater. Trans. B*, 2016, vol. 47, pp. 2411–20.
8. Y. Murakami, S. Kodama, and S. Konuma: *Int. J. Fatigue*, 1989, vol. 11, pp. 291–98.
9. J. Li, G. Cheng, Q. Ruan, J. Pan, and X. Chen: *Metall. Mater. Trans. B*, 2018, vol. 49, pp. 2357–69.
10. J.H. Park, S.B. Lee, and H.R. Gaye: *Metall. Mater. Trans. B*, 2008, vol. 39, pp. 853–61.
11. J.H. Park and Y. Kang: *Steel Res. Int.*, 2017, vol. 88, p. 1700130.
12. J.H. Park and H. Todoroki: *ISIJ Int.*, 2010, vol. 50, pp. 1333–46.
13. J. Li, G. Cheng, Q. Ruan, J. Pan, and X. Chen: *Metall. Mater. Trans. B*, 2019, vol. 50, pp. 2769–79.
14. X. Chen, G. Cheng, Y. Hou, and J. Li: *Metall. Res. Tec.*, 2019, vol. 116, p. 619.
15. C.W. Seo, S.H. Kim, S.K. Jo, M.O. Suk, and S.M. Byun: *Metall. Mater. Trans. B*, 2010, vol. 41, pp. 790–97.
16. Y. Ren, L. Zhang, W. Fang, S. Shao, J. Yang, and W. Mao: *Metall. Mater. Trans. B*, 2016, vol. 47, pp. 1024–34.

17. M. Valdez, G.S. Shannon, and S. Sridhar: *ISIJ Int.*, 2006, vol. 46, pp. 450–57.
18. H. Yang, J. Ye, X. Wu, Y. Peng, Y. Fang, and X. Zhao: *Metall. Mater. Trans. B*, 2016, vol. 47, pp. 1435–44.
19. H.Y. Tang, Y. Wang, G.H. Wu, P. Lan, and J.Q. Zhang: *J. Iron Steel Res. Int.*, 2017, vol. 24, pp. 879–87.
20. Y. Ji, C. Liu, Y. Lu, H. Yu, F. Huang, and X. Wang: *Metall. Mater. Trans. B*, 2018, vol. 49, pp. 3127–36.
21. J.H. Shin and J.H. Park: *ISIJ Int.*, 2018, vol. 58, pp. 88–97.
22. J.S. Park and J.H. Park: *Metall. Mater. Trans. B*, 2016, vol. 47, pp. 3225–30.
23. J.S. Park and J.H. Park: *Metall. Mater. Trans. B*, 2014, vol. 45, pp. 953–60.
24. M. Jiang, X. Wang, B. Chen, and W. Wang: *ISIJ Int.*, 2010, vol. 50, pp. 95–104.
25. J.H. Park and D.S. Kim: *Metall. Mater. Trans. B*, 2005, vol. 36, pp. 495–502.
26. J.W. Kim, S.K. Kim, D.S. Kim, Y.D. Lee, and P.K. Yang: *ISIJ Int.*, 1996, vol. 36, pp. S140–43.
27. J. Li and G. Cheng: *ISIJ Int.*, 2019, vol. 11, pp. 2013–23.
28. Q. Wang, L. Wang, J. Zhai, J. Li, and K.C. Chou: *Metall. Mater. Trans. B*, 2017, vol. 48, pp. 564–72.
29. M. Jiang, X. Wang, and W. Wang: *Ironmak. Steelmak.*, 2012, vol. 39, pp. 20–25.
30. G. Okuyama, K. Yamaguchi, S. Takeuchi, and K.I. Sorimachi: *ISIJ Int.*, 2000, vol. 40, pp. 121–28.
31. Y. Wang, M.K. Oh, T.S. Kim, A. Karasev, W.Z. Mu, J.H. Park, and P.G. Jönsson: *Metall. Mater. Trans. B*, 2021, <https://doi.org/10.1007/s11663-021-02296-2>.
32. G.Y. Qian, F. Jiang, G.G. Cheng, and C.S. Wang: *Metall. Res. Tech.*, 2014, vol. 111, pp. 229–37.
33. X.R. Chen, G.G. Cheng, Y.Y. Hou, J.Y. Li, and J.X. Pan: *J. Iron Steel Res. Int.*, 2020, vol. 27, pp. 913–21.
34. J.H. Park, S.B. Lee, D.S. Kim, and J.J. Pak: *ISIJ Int.*, 2009, vol. 49, pp. 337–42.
35. X. Zhang, B. Xie, H. Li, J. Diao, and C. Ji: *Ironmak. Steelmak.*, 2013, vol. 40, pp. 282–89.
36. L. Zhu, Y. Jia, Z. Liu, C. Zhang, X. Wang, and P. Xiao: *High Temp. Mater. Process.*, 2018, vol. 37, pp. 665–74.
37. D. Hou, Z.H. Jiang, Y.W. Dong, Y. Li, W. Gong, and F.B. Liu: *Metall. Mater. Trans. B*, 2017, vol. 48, pp. 1885–97.
38. K. Suzuki, S. Ban-Ya, and M. Hino: *ISIJ Int.*, 2001, vol. 41, pp. 813–17.
39. M. Hino and K. Ito: *The 19th Committee on Steelmaking*, Tohoku University Press, Sendai, 2010.
40. T. Itoh, T. Nagasaka, and M. Hino: *ISIJ Int.*, 2000, vol. 40, pp. 1051–58.
41. C. Liu, X. Liu, X. Yang, H. Zhang, and M. Zhong: *Metals*, 2019, vol. 9, p. 998.
42. J.J. Pak, J.O. Jo, S.I. Kim, W.Y. Kim, T.I. Chung, S.M. Seo, J.H. Park, and D.S. Kim: *ISIJ Int.*, 2007, vol. 47, pp. 16–24.
43. J.H. Park, S.B. Lee, and D.S. Kim: *Metall. Mater. Trans. B*, 2005, vol. 36, pp. 67–73.

Publisher's Note Springer Nature remains neutral with regard to jurisdictional claims in published maps and institutional affiliations.